Efficient Extraction and Specification-Compliant Optimization of Railway Alignment Parameters from UAV LiDAR Point Clouds

Zhaochen Han, Xuming Ge*, Min Chen, Han Hu

Faculty of Geosciences and Engineering, Southwest Jiaotong University, 611756, Chengdu, China
hanzhaochen@my.swjtu.edu.cn; xuming.ge@swjtu.edu.cn; minchen@home.swjtu.edu.cn; han.hu@swjtu.edu.cn

Keywords: UAV LiDAR point clouds, Track centerline extraction, Railway alignments, Specification, Optimization.

Abstract

The rapid acquisition of high-precision parametric railway alignment is a fundamental prerequisite for intelligent railway construction and maintenance. Traditional measurement techniques and alignment fitting methods heavily rely on manual operations, often resulting in inefficiency, high costs, and insufficient accuracy control. To address these challenges, this study proposes an automated method for extracting and optimizing railway alignment from UAV LiDAR point clouds. Initially, the track centerline is extracted by leveraging the geometric smoothness of the railway and the structural characteristics of the track. A multi-constraint energy model integrating distance, orientation, and curvature is constructed to fit the geometric parameters of alignment elements, thereby providing high-quality initial values for subsequent alignment engineering parameter optimization. Finally, a global optimization strategy based on the simulated annealing algorithm is applied to jointly refine the engineering parameters of the standardized alignment composition, ensuring strict compliance with railway design specification. Experimental results demonstrate that the proposed method can efficiently and robustly extract high-precision alignment parameters with well-defined engineering semantics from complex railway point clouds, thereby providing reliable technical support for intelligent construction and full lifecycle management of railway systems.

1. Introduction

High-precision parametric railway alignment is fundamental to intelligent construction and lifecycle management in railway engineering. Traditional methods, which rely on manual surveying to collect discrete sample points, are inefficient, costly, and incapable of generating a continuous geometric representation of the alignment. Crucially, they fail to directly output the parametric alignment elements required for design and monitoring analysis (Zhou et al., 2021).

The advent of laser scanning technology has transformed data acquisition, enabling the rapid, non-contact capture of dense 3D point clouds at centimeter to millimeter level accuracy (Holgado et al., 2015). Despite this wealth of data, the efficient and accurate extraction of structured, regulation-compliant alignment parameters from massive, unordered, and complex point clouds remains a significant challenge. The specific difficulties are threefold:

(1) The complexity of semantic recognition: Tracks are often occluded and mixed with other structures like ballast and sleepers, making it difficult to isolate key points that define the track centerline.

(2) The standardization of parametric modeling: While polynomial or spline fitting can produce visually smooth curves, their mathematical forms are fundamentally incompatible with the standard 'tangent–transition–circular–transition–tangent' sequence used in railway design (Tong et al., 2010), preventing the direct derivation of engineering parameters such as curve radius and transition length.

(3) The accuracy of alignment segmentation: Imprecise transition points between adjacent alignment segments can cause considerable deviations in the final engineering parameters, even when fitting with design-standard mathematical models.

Although extensive research exists on road alignment extraction from point clouds (Zhou et al., 2021; Ma et al., 2024), the methods are not directly transferable to railways because of systematic differences in engineering scenarios, design standards, and accuracy requirements. To overcome these limitations, this paper proposes a novel framework for the efficient extraction and optimization of railway alignment from UAV LiDAR point clouds. Our main contributions are:

(1) By leveraging the inherent geometric smoothness of railway alignments and the structural characteristics of the track, the proposed method effectively suppresses strong noise and compensates for uneven point density in UAV point clouds, thereby enabling the accurate extraction of a high-precision railway track centerline.

(2) A concise and efficient optimization method for railway alignment engineering parameters is proposed in accordance with railway design specifications. The method effectively mitigates the degradation of parameter accuracy caused by imprecise segmentation of alignment elements. By minimizing a multi-constraint energy function, high-quality initial engineering parameters are obtained, which substantially reduce the parameter search space and significantly improve the efficiency and stability of the optimization process.

2. Related work

2.1 Railway Centerline Extraction

Traditional methods for track centerline extraction are heavily reliant on manual measurement techniques, which are not only labor-intensive but also highly inefficient. While the use of track measurement instruments has significantly enhanced automation and measurement efficiency, these instruments are still susceptible to errors due to various sources of instrument-related inaccuracies. Moreover, when these data are fused, error accumulation becomes more pronounced. In contrast, three-dimensional laser scanning technology offers the ability to rapidly and non-contact capture extensive point cloud data of railways and their surrounding environments with precision on the order of centimeters, or even millimeters. This technology

This contribution has been peer-reviewed. The double-blind peer-review was conducted on the basis of the full paper.
https://doi.org/10.5194/isprs-annals-XI-2-2026-101-2026

enables the high-precision, automated, and continuous extraction of track centerline, thus greatly improving operational efficiency. Beger et al. (2011) introduced a structural recognition framework based on mobile laser scanning point clouds, which, by combining ultra-high-resolution aerial imagery and LiDAR data, facilitates the automatic reconstruction of railway centerline. Pu et al. (2011) developed a feature-based knowledge base for railway objects to support track extraction. Shankar et al. (2020) investigated the integration of Global Navigation Satellite Systems (GNSS), Inertial Measurement Units (IMU), and laser scanners for track centerline extraction. Currently, deep learning methods are predominantly applied to semantic segmentation of point clouds in railway scenarios (Jiang et al., 2023; Wang et al., 2023), but they are not yet capable of directly achieving high-precision track centerline extraction.

While these methods predominantly utilize mobile laser scanning point clouds, which require on-track data collection, their practical efficiency is often constrained by the limited duration of railway maintenance "time windows." In this regard, UAV LiDAR point clouds offer distinct advantages.

2.2 Railway Alignment Modeling

Curve fitting-based techniques offer intuitive mathematical models and facilitate effective visualization. Ma et al. (2019) utilized cubic splines to fit point clouds of road markings according to road design and construction standards, generating alignments capable of achieving navigation and positioning accuracy at a 15-centimeter level. Although spline-based reconstructions produce smooth alignments, they often fail to meet design standards and specifications, limiting their application in final acceptance evaluations, as well as in reconstruction and expansion projects (Garach et al., 2014).

Alignment extraction methods grounded in design standards strictly adhere to railway design specifications, defining the railway alignment as a combination of different parameterized curve elements. Holgado et al. (2015) presented a method for automatically extracting parameterized horizontal alignments from point clouds using bearing intersections and curvature. However, this approach requires user-defined thresholds for scan angles and marking detection intensity, making it sensitive to point cloud noise and requiring manual intervention, which hinders its robustness. In contrast, model-driven methods effectively reduce the impact of noise. Martín et al. (2018) employed the RANSAC algorithm (Fischler et al., 1981) to first extract circular curves from the road centerline, followed by fitting straight lines to the remaining points to extract tangent elements, ultimately classifying the residual points as transition curves. However, RANSAC-based models face challenges in selecting appropriate distance thresholds, which can compromise their stability. Zhou et al. (2021) and Ma et al. (2024) employed mathematical models from railway design standards for global fitting of geometric parameters across various alignment elements using an energy function. While this method can relatively accurately estimate the geometric parameters of different elements, the precision of engineering parameters derived from these geometric values diminishes due to imprecise segmentation of element types. Li et al. (2018) optimized alignment engineering parameters using a PSO-based algorithm, but the method lacks sufficient local refinement capability, resulting in limited optimization accuracy. Yang et al. (2026) employed a nested PSO-MADS algorithmic framework, leading to high computational complexity and low optimization efficiency.

To overcome the drawbacks of the aforementioned approaches, this study introduces a multi-constraint energy function to obtain high-quality initial alignment parameters, thereby significantly narrowing the parameter search space. Building upon these initial values, a simulated annealing algorithm with integrated global exploration and local refinement capabilities is employed to efficiently and reliably determine the optimal engineering parameters.

3. Methodology

As illustrated in Figure 1, the proposed method involves three key steps. First, the track centerline is extracted based on the geometric smoothness of the railway alignment and the structural characteristics of the track. Next, a multi-constraint energy model integrating distance, orientation, and curvature is constructed to fit the geometric parameters of alignment elements, thereby providing high-quality initial values for subsequent alignment engineering parameter optimization. Finally, a simulated annealing global optimization algorithm is employed to jointly optimize the track alignment parameters, yielding high-precision parameters with clear engineering semantics, which can be directly applied in railway design.

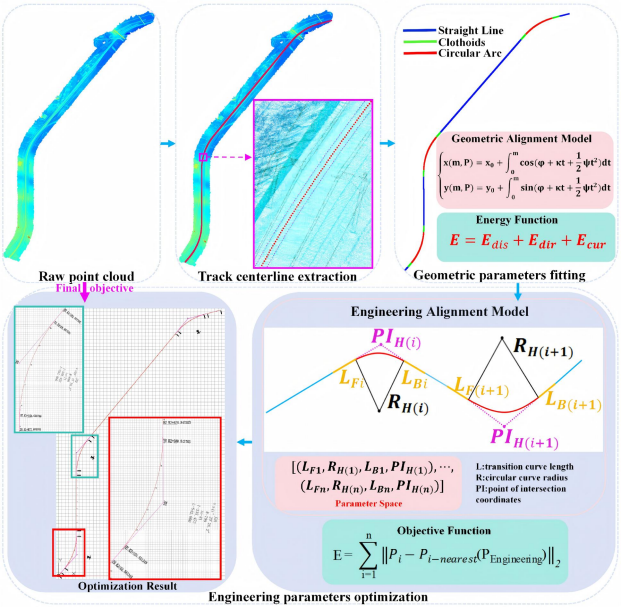

Figure 1. Workflow.

3.1 Railway track centerline extraction

Based on the geometric smoothness and structural characteristics of railway tracks, this study proposes an automatic seed point growth method for extracting track centerlines by efficiently and robustly acquiring rail top surface center points.

The method begins by selecting two adjacent points (approximately 2 meters apart) on the top surface of a single rail as initial seed points P_1 and P_2. The line connecting these two points defines the initial local coordinate system for the directional growth process. Compared with mobile laser scanning data, UAV LiDAR point clouds of rail tops often exhibit significant noise and uneven point density. To address this, the rail design height is used as the search radius to extract all points within the spherical neighborhoods of P_1 and P_2. Points whose elevation differs from the highest point in the neighborhood by 3 cm (i.e., the rail top thickness) are identified as rail top candidate points. If the elevation of the current highest point deviates from the mean elevation of all candidate

This contribution has been peer-reviewed. The double-blind peer-review was conducted on the basis of the full paper.
https://doi.org/10.5194/isprs-annals-XI-2-2026-101-2026 | © Author(s) 2026. CC BY 4.0 License.

points by more than 3 standard deviations, it is considered noise and removed, and the highest point is reselected until the criteria are met. The elevation of the finalized highest point and the planar arithmetic mean coordinates of the corresponding candidate points are then assigned to the seed point, completing its accurate calibration.

Using the calibrated seed points P_1 and P_2, the direction vector $V = P_2 - P_1$ is calculated. After normalization, this vector represents the local tangential direction of the rail. The automatic growth of seed points for both left and right rails is implemented through the following steps:

a. Step Prediction: Starting from the current seed pair, new seed points P_3 and P_4 are predicted by moving forward along the unit direction vector with a preset step length L.

b. Centroid Correction: To account for potential deviations caused by rail curvature, elevation changes, or point cloud noise, the predicted points P_3 and P_4 are adjusted using the same calibration method applied to the initial seed points.

c. Iteration and Data Association: The corrected point pair (P_3, P_4) serves as the new current seed points, and steps a and b are repeated. Each calibrated seed point is added to the set of top-surface centerline points, continuing until the full point cloud for that rail has been processed. The same growth procedure is applied independently to the opposite rail.

After seed point growth is completed, a k-d tree is constructed from the seed point data of both left and right rail top surfaces. For each point in the left rail seed set, its spatial nearest neighbor in the right rail set is rapidly identified using the k-d tree. The track center point is calculated as $P_{center} = (P_{left}+P_{right}) / 2$. Finally, all track center points are sequentially connected along the direction of the track to generate a continuous 3D vector track centerline.

3.2 Geometric Parameters Fitting for Alignment

To generate high-quality initial values for optimizing railway alignment engineering parameters, this study applies a multi-constraint energy minimization function, formulated under railway track design standards and incorporating distance, direction, and curvature cues.

3.2.1 Geometric Alignment Model

According to railway design standards, a railway alignment consists of a sequence of elements, including straight lines, transition curves, and circular arcs. The mathematical formulation is given in Equation (1). After reconstructing the horizontal alignment, the reconstruction of vertical curves becomes a straightforward regression problem (Zhou et al., 2021). Therefore, the focus is placed on the horizontal alignment.

$$\begin{cases} X(m) = X_0 + \int_0^m \cos\left(\varphi + \kappa t + \frac{1}{2}\psi t^2\right) dt \\ Y(m) = Y_0 + \int_0^m \sin\left(\varphi + \kappa t + \frac{1}{2}\psi t^2\right) dt \\ Z(m) = Z_0 + \xi m + \frac{1}{2}\eta m^2 \end{cases} \quad (1)$$

where m denotes the 2D curve length from (X_0, Y_0) to (X(m), Y(m)) after projecting the 3D curve onto the horizontal plane, and $P_{Geometric}=\{\varphi,\kappa,\psi\}$ represents the geometric parameters of the horizontal alignment elements.

3.2.2 Geometric Parameters Fitting

In mathematical terms, the curvature of a straight line segment is zero, while the curvature of a circular arc segment is constant, defined as the reciprocal of the radius. The curvature of a transition curve lies between zero and that of a circular arc, serving to smoothly connect the straight line and circular arc segments. Therefore, in this study, we first calculate the curvature of the entire railway alignment's track center points. Based on a curvature threshold, we classify the candidate points for the straight line and circular arc segments. Then, we apply the RANSAC algorithm to fit the points within each candidate set of straight line and circular arc segments. Finally, the remaining points are classified as transition curve points (Martín et al., 2018).

Due to the small curvature variation at the transition between different alignment segments and the difficulty in determining the distance threshold for the RANSAC algorithm, the accuracy of segment classification is limited. This, in turn, affects the precision of the derived engineering parameters. To address this issue, this study introduces a global optimization strategy based on simulated annealing to jointly optimize the engineering parameters of the railway alignment that comply with design standards.

To fit the geometric parameters of the railway alignment with high precision, thereby providing high-quality initial values for subsequent engineering parameter optimization and reducing the parameter search space of non-convex optimization, we employ a multi-constraint energy function minimization method that integrates distance, direction, and curvature. This method iteratively adjusts parameters to fit the curve, aiming to minimize the discrepancy between predicted data points and actual data points, thus improving the accuracy of the model in representing the real railway alignment (Gálvez et al., 2013). The multi-constraint energy function is defined as (Ma et al., 2024):

$$E = E_{distance} + E_{direction} + E_{curvature} \quad (2)$$

the individual components are:

$$E_{distance} = \sum_{i=1}^{n}\sum_{j=1}^{s} \left\| P_{i,j} - P(m_{i,j}, P_{Geometric-i}) \right\|_2 \quad (3)$$

$$E_{direction} = \sum_{i=2}^{n}\sum_{j=1}^{s} (Mdir_0^{i-1} - \varphi^i)^2 + (Mdir_1^{i-1} - \widehat{\varphi}^i)^2 \quad (4)$$

$$E_{curvature} = \sum_{i=1}^{n-1}\sum_{j=1}^{s} \left| \kappa^i + m_{i,j}\psi^i - \kappa^{i+1} \right| \quad (5)$$

where n represents the number of segmented curve elements, and s denotes the number of points within each segment. The parameters $Mdir_0^{i-1}$ and $Mdir_1^{i-1}$ represent the main directions of the start and end points of the $(i-1)$-th segment, respectively. The variable φ^i represents the direction of the curve, and κ^i represents its curvature.The expression $\widehat{\varphi}^i=\varphi^i+\kappa^i m_{i,j}+\frac{1}{2}\psi^i m_{i,j}^2$ indicates that the curve direction is adjusted by its curvature and the rate of change of curvature over the segment length, where $m_{i,j}$ is the cumulative mileage of the i-th curve element and ψ^i represents the change rate of the horizontal curvature. The main direction is calculated using Principal Component Analysis (PCA) within a specified point neighborhood.

3.3 Engineering Parameters Optimization for Alignment

Although the proposed method effectively fits the geometric parameters of various alignment elements, the segmentation

accuracy is limited by the relatively small curvature variations at transition points and the difficulty in determining an optimal distance threshold for the RANSAC algorithm. This results in a noticeable reduction in the precision of the engineering parameters derived from the geometric alignment data in the railway design process. To overcome these challenges, this study computes the initial engineering parameters based on the derived geometric alignment parameters and incorporates a global optimization strategy based on simulated annealing to jointly optimize the engineering parameters of the standardized alignment model. This approach effectively addresses the issue of low segmentation accuracy among different alignment types, ultimately yielding high-precision railway alignment parameters with clear engineering significance.

3.3.1 Engineering Alignment Model

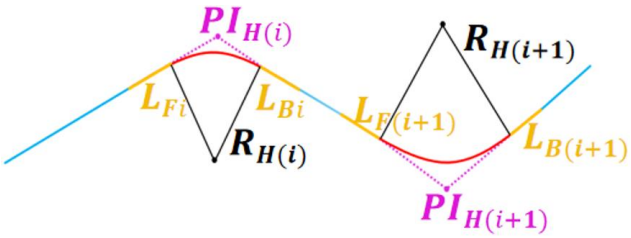

Figure 2. Alignment Engineering Parameters Model.

The railway alignment typically consists of a sequence of standardized alignment elements, as shown in Figure 2, including straight lines, transition curves and circular arcs (FSDI, 2017). The steps for generating the standardized railway alignment using the intersection method are as follows:

1. Compute the inward displacement p and the tangent correction q for the transition curves using equations (6), respectively:

$$\begin{cases} p = \dfrac{L_s^2}{24R} \\ q = \dfrac{L_s}{2} - \dfrac{L_s^3}{240R^2} \end{cases} \tag{6}$$

where L_s is the length of the transition curve, and R is the radius of the circular arc.

2. Determine the lengths of the tangent lines T1 and T2 as shown in equation (7):

$$T = (R+p)\tan\left(\frac{|\Delta|}{2}\right) + q \tag{7}$$

3. Calculate the split points $TS(X_{TS}, Y_{TS})$ and $ST(X_{ST}, Y_{ST})$ between the straight line and the transition curve, using equation (8):

$$\begin{cases} TS = PI - T1 \cdot t_1 \\ ST = PI + T2 \cdot t_2 \end{cases} \tag{8}$$

where t_1 and t_2 are the unit vectors in the direction of the front and rear tangents, respectively.

4. Compute the split points $SC(X_{SC}, Y_{SC})$ and $CS(X_{CS}, Y_{CS})$ between the circular arc and the transition curve. The equation for generating the transition curve points is given by:

$$\begin{cases} x(l) = l - \dfrac{l^5}{40A^4} + \dfrac{l^9}{3456A^8} \\ y(l) = \dfrac{l^3}{6A^2} - \dfrac{l^7}{336A^6} \end{cases} \tag{9}$$

where $l \in [0, L_s]$ and $A = \sqrt{R \cdot L_s}$.

The transition curve points are then transformed from local coordinates to the tangent direction, as described in equations (10):

$$\begin{cases} P_{entry} = TS + x \cdot t_1 + y \cdot n_1 \\ P_{exit} = ST - x \cdot t_2 + y \cdot n_2 \end{cases} \tag{10}$$

where n_1 and n_2 are the unit vectors in the direction of the front and rear tangents, respectively, and their directions align with the deflection of the transition curve.

The points SC and CS are the endpoints of the front and rear transition curves, and the transition curve lengths L_{s1} and L_{s2} are substituted into equations (10) to determine $SC(X_{SC}, Y_{SC})$ and $CS(X_{CS}, Y_{CS})$.

5. Generate the points for the circular arc using equation (11):

$$P = O + R \cdot (\cos\theta, \sin\theta) \tag{11}$$

where $\theta = \theta_{SC} + isCCW \cdot \frac{s}{R}$, s is the length of the circular arc, the center $O = SC + R \cdot n_{SC}$, and $n_{SC} = (-\sin\theta_{SC}, \cos\theta_{SC})$ is the normal vector at SC. The angle θ_{SC} is the tangent direction at the transition point, defined as $\theta_{TS} + \beta_0$, where θ_{TS} is the direction of the front tangent, and the curve angle $\beta_0 = \frac{L_s}{2R}$. When the arc deviates counterclockwise, $isCCW = +1$, and when it deviates clockwise, $isCCW = -1$.

6. Based on the forward direction of the railway line, the alignment elements generated in the previous steps are sequentially connected to form the complete railway alignment.

Given the limited segmentation accuracy of the alignment method presented in Section 3.2, directly applying the derived geometric parameters to regenerate the railway alignment according to the above procedure would markedly compromise the overall precision. Therefore, this study performs a joint optimization of the critical engineering parameters of the alignment model to enhance geometric consistency and design accuracy. As shown in Figure 2, the parameter set is defined as $P_{Engineering}$: $[(L_{F1}, R_{H(1)}, L_{B1}, PI_{H(1)}), \cdots, (L_{Fn}, R_{H(n)}, L_{Bn}, PI_{H(n)})]$, where L represents the length of the transition curve, R represents the radius of the circular curve, and PI represents the coordinates of the intersection point.

3.3.2 Engineering Parameters Optimization

The optimization process aims to minimize the planar distance between the extracted track center points and the alignment generated from the predicted values of the engineering parameters $P_{Engineering}$. This ensures that the optimized alignment not only strictly conforms to the standardized railway design model of tangent – transition – circular – transition – tangent, but also achieves the best possible fit to the actual track centerline derived from point-cloud data. The objective function is defined as follows:

$$E = \sum_{i=1}^{n} \left\| P_i - P_{i-nearest}(P_{Engineering}) \right\|_2 \tag{12}$$

where P_i denotes the i-th track center point, $P_{i\text{-}nearest}(P_{Engineering})$ represents the nearest point on the

alignment generated by the engineering parameters $P_{Engineering}$, and n is the total number of track center points.

During optimization, the geometric parameters $P_{Geometric}$ obtained from the multi-constraint energy model fitting are used to compute high-quality initial values for $P_{Engineering}$, thereby reducing the parameter search space of the non-convex optimization problem. Based on the Metropolis–Hastings sampling mechanism (Andrieu et al., 2003), new candidate solutions are intelligently proposed within the feasible parameter space, while a simulated annealing framework governs the optimization process. In the early stages, a higher “temperature” is adopted to probabilistically accept certain inferior solutions, enhancing global exploration capability and avoiding local minima. As the iterations proceed, the temperature gradually decreases according to a predefined schedule, shifting the focus toward local refinement until convergence to the global optimum is achieved (Wu et al., 2025).

This global optimization strategy effectively alleviates the loss of precision in alignment engineering parameters, including circular arc radii, transition curve lengths, and tangent azimuths, which can result from segmentation inaccuracies.

4. Experiment and analysis

4.1 Experimental data

In this study, two UAV LiDAR point cloud datasets were employed for experimental validation: dataI from Qinghai Province (approximately 5 km) and dataII from Guizhou Province (approximately 3 km), China. Both datasets encompass various alignment configurations, including tangents, transition curves, and circular arcs, with point cloud densities of approximately 2000 pts/m ^{2}, providing excellent spatial coverage and rich geometric detail. These characteristics make the datasets particularly suitable for high-precision extraction and optimization of railway track centerline and alignment parameters. The experimental datasets are illustrated in Figure 3.

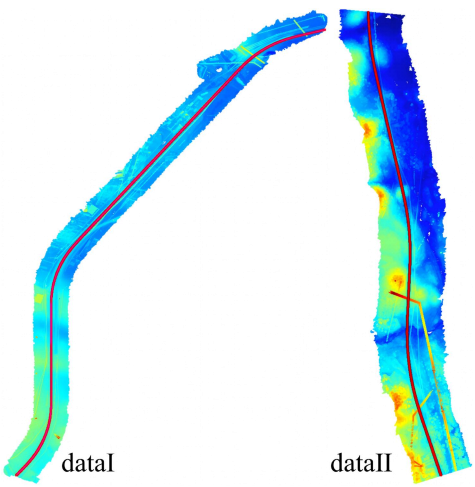

Figure 3. UAV point cloud datasets.

4.2 Experimental results and evaluation

4.2.1 Qualitative Evaluation

The proposed method exhibits strong robustness and adaptability in complex railway environments. As shown in Figure 4, the red dots represent manually surveyed track center points, the pink lines correspond to the railhead centerline, and the yellow line denotes the extracted track centerline. It can be observed that the method effectively identifies the left and right railhead centerline even at railway turnouts, producing a continuous and smooth track centerline.

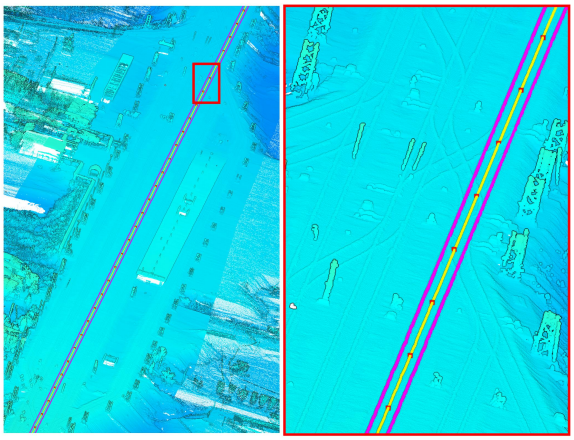

Figure 4. Results of track centerline extraction.

Furthermore, the results of railway alignment extraction and optimization are presented in Figure 5. The optimized alignment strictly adheres to the standardized railway design model composed of tangent–transition–circular–transition–tangent elements and closely fits the track center points extracted from the original point cloud data. These outputs can be directly applied to railway design and related engineering applications.

4.2.2 Quantitative Evaluation

To objectively evaluate the accuracy of the proposed method, quantitative analyses were conducted for both the extracted track center points and the optimized alignment results.

By comparing the extracted track center points with manually surveyed reference points, the elevation and planar displacement deviations were statistically analyzed. As shown in Figure 6, the elevation deviations are primarily concentrated within ±2 cm, while most planar displacements are less than 3 cm, indicating that the proposed track center point extraction method achieves high accuracy and stability.

As defined in Equation (13), the root mean square error (RMSE) of alignment offsets was used as an evaluation metric to assess the fitting performance between the alignment and the track center points before and after optimization.

$$\mathrm{RMSE}_{\mathrm{shift}} = \sqrt{\frac{1}{N}\sum_{i=1}^{N} \left\| P_i - P_{i-nearest}(\mathrm{P}_{\mathrm{Engineering}}) \right\|_2} \qquad (13)$$

where P_i denotes the extracted track center point, $P_{i\text{-}nearest}(\mathrm{P}_{\mathrm{Engineering}})$ represents the nearest point on the alignment generated from the engineering parameters $\mathrm{P}_{\mathrm{Engineering}}$, and N is the total number of track center points.

This contribution has been peer-reviewed. The double-blind peer-review was conducted on the basis of the full paper.
https://doi.org/10.5194/isprs-annals-XI-2-2026-101-2026 | © Author(s) 2026. CC BY 4.0 License.

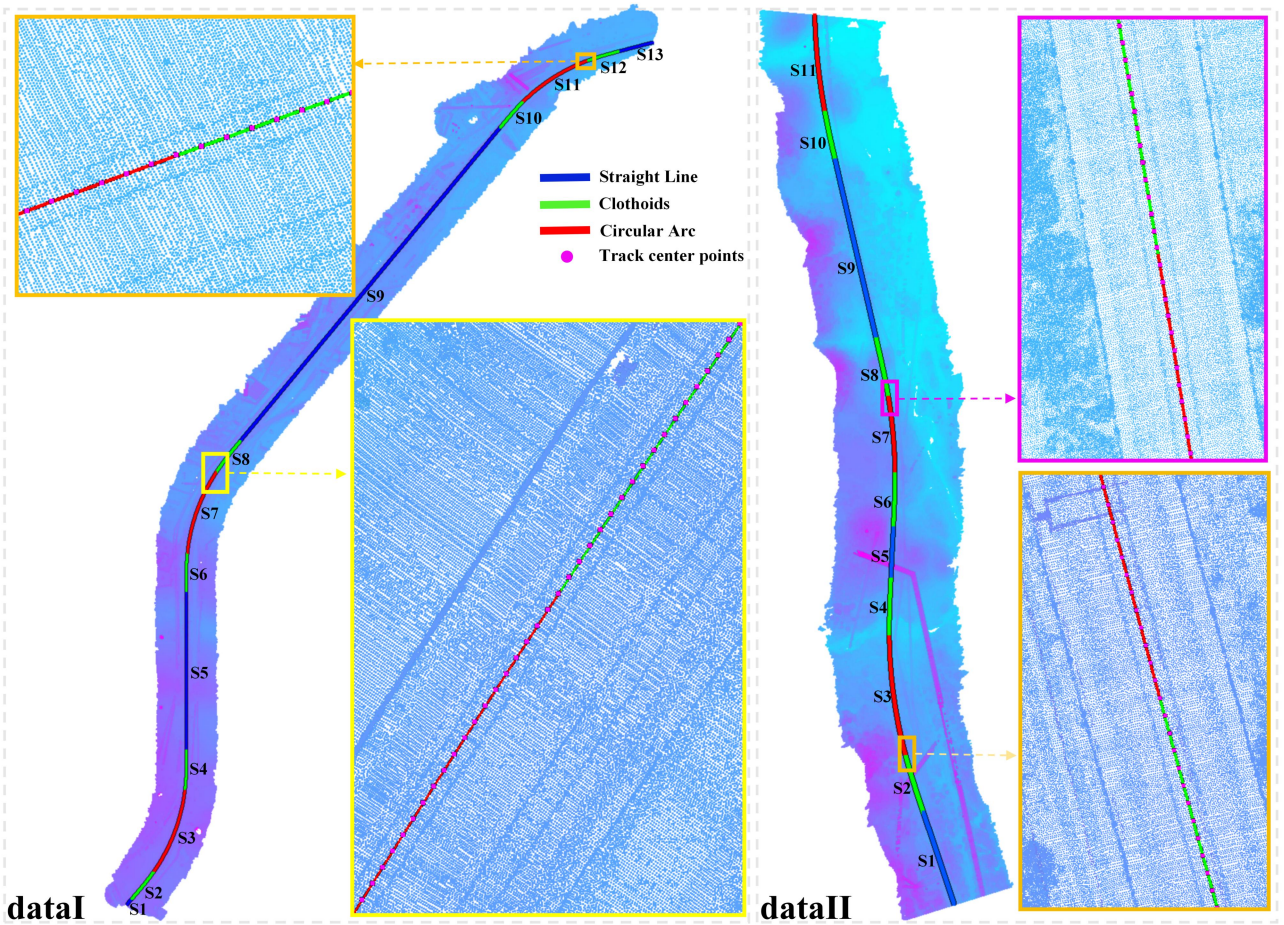

Figure 5. Results of alignments extraction and optimization.

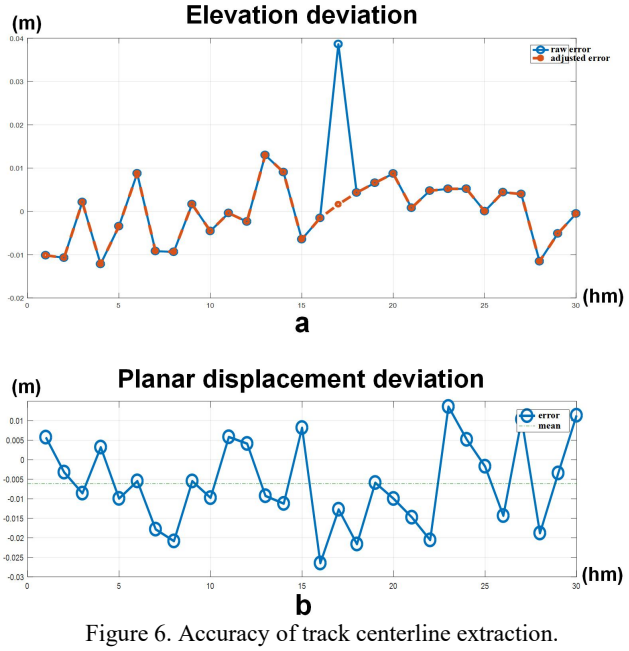

Figure 6. Accuracy of track centerline extraction.

As summarized in Table 1, the proposed method is evaluated on two datasets (dataI and dataII) and compared against the baseline method (Ma et al., 2024). For dataI, the RMSE of alignment offsets across all test sections ranges from 0.0154 m to 0.0397 m, significantly outperforming the baseline method, which yields RMSE values between 0.0446 m and 0.2785 m. Similarly, for dataII, the proposed method achieves RMSE values between 0.0129 m and 0.0442 m, compared to the baseline's range of 0.0571 m to 0.1942 m. The substantial improvement in accuracy across all sections verifies the effectiveness of the proposed optimization strategy.

Section	dataI (Ma et al., 2024)	dataI (Ours)	dataII (Ma et al., 2024)	dataII (Ours)
S1	0.0753	0.0201	0.0639	0.0129
S2	0.2643	0.0297	0.1942	0.0196
S3	0.2272	0.0285	0.1521	0.0183
S4	0.1909	0.0252	0.1684	0.0442
S5	0.0446	0.0213	0.0765	0.0253
S6	0.1746	0.0269	0.1347	0.0157
S7	0.2785	0.0301	0.1836	0.0201
S8	0.1126	0.0358	0.0952	0.0186
S9	0.0537	0.0325	0.0571	0.0146
S10	0.1203	0.0397	0.1873	0.0196
S11	0.2548	0.0259	0.1625	0.0282
S12	0.2255	0.0276	-	-
S13	0.0541	0.0154	-	-

Table 1. Simulated annealing optimization comparison (RMSE).

4.3 Performance Analysis

4.3.1 Railway track centerline extraction

Leveraging the geometric smoothness of railway alignments and the structural characteristics of the track, the proposed rail top surface seed-point growth method demonstrates strong robustness and efficiency in extracting high-precision track center points, even in sparse point cloud regions or complex turnout areas. This capability ensures stable performance under challenging conditions and provides a reliable data foundation for subsequent railway alignment extraction and optimization.

4.3.2 Multi-Constraint Energy Model

The accuracy of geometric parameter fitting for alignment elements directly affects the efficiency and convergence of subsequent engineering parameter optimization. By minimizing the proposed multi-constraint energy model that integrates distance, direction, and curvature constraints, the method provides high-quality initial parameters, which in turn accelerate the convergence of the optimization process. As shown in Figure 7 (b) and (d), the fitting results obtained without these constraints exhibit noticeable discontinuities at alignment junctions. In comparison, the multi-constraint energy model, as illustrated in Figure 7 (a) and (c), produces a smooth and continuous alignment that effectively balances data fidelity and geometric smoothness.

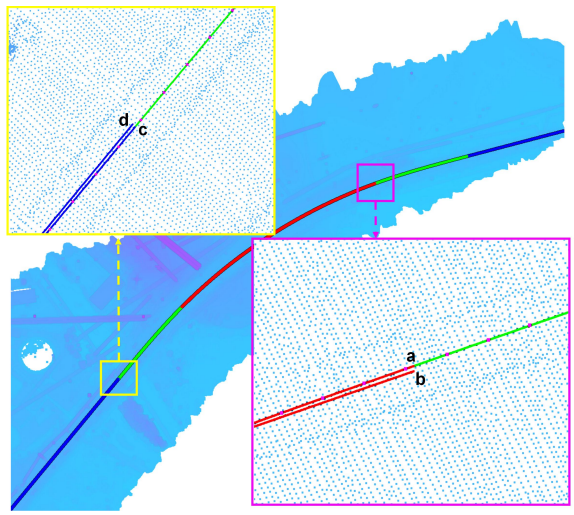

Figure 7. Performance of multi-constraint energy model.

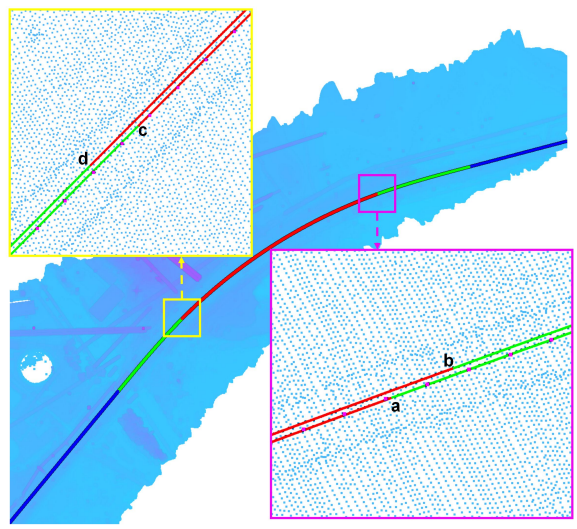

Figure 8. Performance of simulated annealing optimization.

4.3.3 Simulated Annealing Optimization

Although the fitted curve in Figure 7 demonstrates close agreement with the track center points, practical railway engineering design employs the intersection method (see Fig. 2) based on alignment engineering parameters to generate the final alignment. Figure 8 (b) and (d) shows the alignment drawn using the initial values of engineering parameters derived from the geometric parameters fitted in Section 3.2. The loss of alignment precision is clearly attributable to imprecise segmentation of different alignment element types.

In other words, the alignment (see Fig. 7 (a) and (c)) generated by the method described in Section 3.2 represents only a mathematical curve-fitting result of alignment elements with imprecise segmentation, rather than a standardized alignment that strictly complies with railway design specifications (see Fig. 2), and thus it is not directly applicable to practical railway engineering design.

As illustrated in Figure 8 (a) and (c), the optimized alignment maintains the standardized design structure while exhibiting a markedly improved fit to the measured track center points. This optimization process effectively addresses engineering parameter deviations arising from inaccurate alignment segmentation and ultimately yields high-precision railway alignment parameters with clear engineering significance.

5. Conclusion

This study presents a fully automated framework for extracting and optimizing railway alignment parameters from UAV LiDAR point clouds. The proposed framework has been validated across representative railway scenarios, demonstrating its ability to identify track structures and extract precise track centerlines by leveraging the geometric smoothness of railway alignments and structural characteristics of tracks. A multi-constraint energy model incorporating distance, direction, and curvature information is then established to obtain high-precision initial geometric parameters for straight lines, transition curves, and circular curves, providing reliable initial values for subsequent engineering parameter optimization. Furthermore, a simulated annealing-based global optimization strategy is introduced to jointly refine the engineering parameters of standardized alignment combinations. The optimized alignments strictly conform to railway design specifications while maintaining explicit engineering semantics, ensuring geometric consistency and practical applicability.

Comprehensive experiments verify that the proposed method achieves robustness, computational efficiency, and high accuracy in complex and noisy point-cloud environments. The framework supports railway design verification, digital twin modeling, and full lifecycle management of high-precision parametric alignments. Overall, the proposed approach provides a reliable and scalable technical foundation for intelligent railway construction, operation, and maintenance, contributing to data-driven and automation-oriented railway engineering.

Acknowledgements

This work was supported by the National Natural Science Foundation of China under Grant 42471484.

References

Andrieu, C., De Freitas, N., Doucet, A., Jordan, M.I., 2003. An introduction to MCMC for machine learning. *Machine Learning*, 50, 5–43.

Beger, R., Gedrange, C., Hecht, R., 2011. Data fusion of extremely high resolution aerial imagery and LiDAR data for automated railroad centre line reconstruction. *ISPRS Journal of Photogrammetry and Remote Sensing*, 66(6), 40-51.

Fischler, M.A., Bolles, R.C., 1981. Random sample consensus - a paradigm for modelfitting with applications to image-analysis and automated cartography. *Commun. ACM*, 24(6), 381–395.

FSDI, 2017. *Code for Railway Line Design*. China Railway Publishing House, Beijing.

Gálvez, A., Iglesias, A., 2013. A new iterative mutually coupled hybrid GA–PSO approach for curve fitting in manufacturing. *Applied Soft Computing*, 13(3), 1491-1504.

Garach, L., Oña, J.d., Pasadas, M., 2014. Mathematical formulation and preliminary testing of a spline approximation algorithm for the extraction of road alignments. *Automation in Construction*, 47, 1-9.

Holgado-Barco, A., González-Aguilera, D., Arias-Sanchez, P., 2015. Semiautomatic extraction of road horizontal alignment from a mobile LiDAR system. *Computer-Aided Civil and Infrastructure Engineering*, 30(3), 217-228.

Jiang, T., Yang, B., Wang, Y., Dai, L., Qiu, B., Liu, S., Li, S., Zhang, Q., Jin, X., Zeng, W., 2023. RailSeg: Learning local-global feature aggregation with contextual information for railway point cloud semantic segmentation. *IEEE Transactions on Geoscience and Remote Sensing*, 61.

Li, F., Ren, X., Luo, W., Chen, X., 2018. Methodology for existing railway reconstruction with constrained optimization based on point cloud data. *Applied Sciences*, 8, 1782.

Ma, L., Li, Y., Li, J., 2019. Generation of Horizontally Curved Driving Lines in HD Maps Using Mobile Laser Scanning Point Clouds. *IEEE Journal of Selected Topics in Applied Earth Observations Remote Sensing*, 12(5), 1572-86.

Ma, R., Zhu, Q., Ge, X., Jia, X., Hu, H., Liu, T., 2024. Precision Inverse Modeling of Highway Pavements Based on Standardized Alignment. *IEEE Journal of Selected Topics in Applied Earth Observations and Remote Sensing*, 17, 11069-11085.

Martín-Jiménez, J.A., Zazo, S., Justel, J.J.A., 2018. Road safety evaluation through automatic extraction of road horizontal alignments from Mobile LiDAR System and inductive reasoning based on a decision tree. *ISPRS Journal of Photogrammetry and Remote Sensing*, 146, 334-346.

Pu, S., Rutzinger, M., Vosselman, G., 2011. Recognizing basic structures from mobile laser scanning data for road inventory studies. *ISPRS Journal of Photogrammetry and Remote Sensing*, 66(6), 28-39.

Shankar, S., Roth, M., Schubert, L.A., 2020. Automatic Mapping of Center Line of Railway Tracks using Global Navigation Satellite System, Inertial Measurement Unit and Laser Scanner. *Remote Sensing*, 12(3), 411.

Tong, X., Meng, X., Ding, K., 2010. Estimating geometric parameters of highways and railways using least-squares adjustment. *Survey Review*, 42(318), 359-374.

Wang, Z., Geng, Y., Jia, L., Yang, F., Chen, Y., Wang, R., Chen, S., 2023. Self-attentive local aggregation learning with prototype guided regularization for point cloud semantic segmentation of high-speed railways. *IEEE Transactions on Intelligent Transportation Systems*, 24(10), 11157-11170.

Wu, S., Chen, C., Yang, B., Yan, Z., Wang, Z., Sun, S., Zou, Q., Fu, J., 2025. PylonModeler: A hybrid-driven 3D reconstruction method for power transmission pylons from LiDAR point clouds. *ISPRS Journal of Photogrammetry and Remote Sensing*, 220, 100-124.

Yang, R., Li, W., Wan, X., Pu, H., Schonfeld, P., Lu, C., Zhang, Z., Peng, L., 2026. A 3D existing railway alignment recreation method based on particle swarm optimization and mesh adaptive direct search. *Expert Systems with Applications*, 299(B), 130199.

Zhou, Y., Huang, R., Jiang, T., Dong, Z., Yang, B., 2021. Highway alignments extraction and 3D modeling from airborne laser scanning point clouds. *International Journal of Applied Earth Observation and Geoinformation*, 102, 102429.

This contribution has been peer-reviewed. The double-blind peer-review was conducted on the basis of the full paper.
https://doi.org/10.5194/isprs-annals-XI-2-2026-101-2026